

The X-ray response of epitaxial GaAs

Alan Owens, M. Bavdaz, S. Kraft, A. Peacock

Space Science Department of ESA, ESTEC, 2200AG Noordwijk, Netherlands

S. Nenonen, H. Andersson, M.A. Gagliardi, T. Gagliardi

Metorex International Oy, P.O. Box 85, FIN-02201 Espoo, Finland

F. Scholze, G. Ulm

Physikalisch-Technische Bundesanstalt, Abbestr. 2-12, D-10587 Berlin, Germany

Abstract

We summarise the results of a number of X-ray experiments on an epitaxial GaAs device carried out in both our laboratory and at the PTB Radiometry Laboratory at the BESSY Synchrotron Radiation Source. The detector has a diameter of 1.5 mm and is fully depleted to a depth of 40 μ m. It has been characterized as a function of energy, bias and temperature. At -35°C we determine the charge collection efficiency to be 97% and find that energy resolutions ranging from 730 to 930eV fwhm can be readily achieved using conventional pre-amplifiers over the energy range 6-60 keV. By considering the various contributions to the fwhm, we show that leakage current and charge trapping noise dominate the resolution function. From detector modelling we determine the effective electron and hole density/cross section products to be 7 and 3 cm⁻¹, respectively.

1. Introduction

In the last decade, gallium arsenide (GaAs) has attracted considerable interest as a viable alternative to Si or Ge for the detection of X-rays above a few keV. It is one of the high group compound semiconductors with a bandgap sufficiently wide (1.42 eV) to permit room temperature operation (for a review, see Buttar [1]) but small enough so that its Fano limited spectroscopic resolution is close to that of Si. The atomic numbers of its constituents bracket that of germanium, thus potentially offering the advantages of a Ge detector, such as high detection efficiency and robustness, without the inherent disadvantage of cryogenic cooling. However, in spite of two decades of intensive research, its potential has not yet been fully realised. Early bulk devices suffered from poor charge collection and intermittent burst noise, and while later devices fabricated by liquid vapour or chemical vapour phase epitaxial deposition techniques proved to be good detectors, they suffered from poor detection efficiencies, due to the difficulties in producing thick layers with low-doping concentrations. At the present time the attainable energy resolution is limited by the high reverse (i.e., leakage) current density of the rectifying junction and the high concentration of trapping centres for electrons and holes.

With recent advances in material sciences [2], there has been renewed interest in detectors based on both bulk and epitaxially grown material - primarily for high energy physics and X-ray astrophysics applications above 10 keV. In this paper, we report the results of a series of experiments to characterise the X-ray response of a GaAs epitaxial detector. Preliminary results have been presented elsewhere [3].

2. Experimental

A 1.5 mm diameter (1.77 mm^2) epitaxial device was used in the present study. It was formed by growing a $40 \mu\text{m}$ intrinsic layer onto a $100 \mu\text{m}$ thick n^+ GaAs wafer by Chemical Vapour Phase Deposition (CVPD). A p-i-n structure is then formed by depositing a $5 \mu\text{m}$ thick p^+ layer directly onto the epitaxial layer and a full wafer ohmic (Au/Ni/Ge/Au) contact deposited on the n^+ side. A cross-sectional view of the device is shown in Figure 1. The p^+ side was patterned by etching to define the detector and a guard ring to minimize surface leakage. Both the mesa and guard ring are metalized with Au/Pt/Ti to form a Schottky contact. The device characteristics are listed in Table 1.

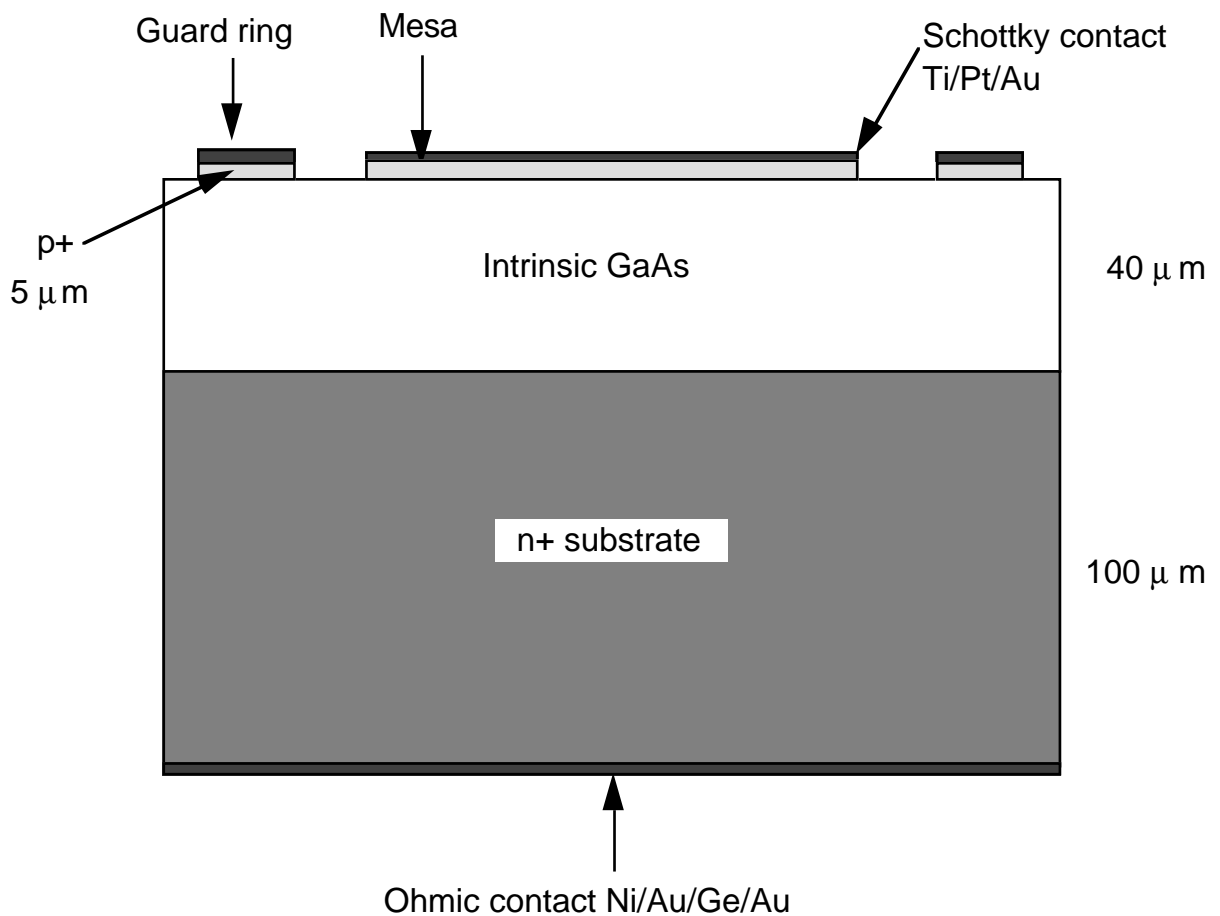


Figure 1. Schematic cross-section of the detector.

Table 1. Device Characteristics

Parameter	Value
Diameter (physical)	1.5 mm
Active area	1.77 mm ²
Depletion depth	40 μ m
Dead layer thickness	5 μ m
Maximum operating bias	-10 V (T=17°C) to -90 V (T= -35°C)
Nominal Bias & operating temperature	-40V, -35°C
Capacitance @ nominal bias	4.4 pF
Leakage current @ nominal bias	0.04 nA
Energy resolution @ 5.9 keV, 20 keV, 59.5 keV	728 eV, 750, 924 eV fwhm @ -35°C
Detection efficiency @ 6.4 keV, 20 keV, 59.5 keV	61%, 52%, 4.5%

The device was operated as a reverse-biased diode with the p⁺ blocking contact at negative potential. At the nominal bias, the 40 μ m epitaxial film is considered to be fully depleted with a very sharp boundary at the conductive n⁺ GaAs substrate. The typical bias and leakage currents were -40V and 0.04 nA, respectively at temperatures < -10°C. The detector was mounted on a two stage peltier cooler. The analog chain consists of a modified PGT P014TR-N preamplifier in conjunction with an Ortec 671 spectroscopy amplifier. Since the system is susceptible to microphonics, the detector was acoustically and vibrationally isolated from its environment and active baseline restoration employed during all measurements.

Figure 2 shows the variation of the measured fwhm energy resolution as a function of shaping time constant measured with an Fe⁵⁵ source. The curve rises sharply at low shaping times due to series noise (i.e., Johnson noise produced in the input FET and biasing components) and more slowly at high shaping times because of increased susceptibility to the shot noise of the leakage current. The solid line shows the expected variation. Based on this curve a shaping time of 3 μ s was used throughout the measurements. Analog output pulses from the amplifier are digitized by a Canberra 8701 ADC and stored and processed by a PC.

The device has been studied at both high and low energies using 2 radioactive sources (Fe⁵⁵ and Am²⁴¹), 6 fluorescent target sources (Cu, Rb, Mo, Ag, Ba and Tb) and the BESSY electron storage ring facility. In the latter case, measurements were carried out on the KMC beamline [4] which utilizes a double crystal monochromator to produce a highly monochromatic X-ray beam. The photon beam energy is variable over the energy range

800 to 5000 eV with a spectral resolving power ($E/\Delta E$) of 1000-2000. The beam is collimated to a spatial extent of 300 μm diameter at the detector. The detector was mounted on a 2 axis translation table allowing the device scanned in X and Y to a precision of $\pm 10 \mu\text{m}$.

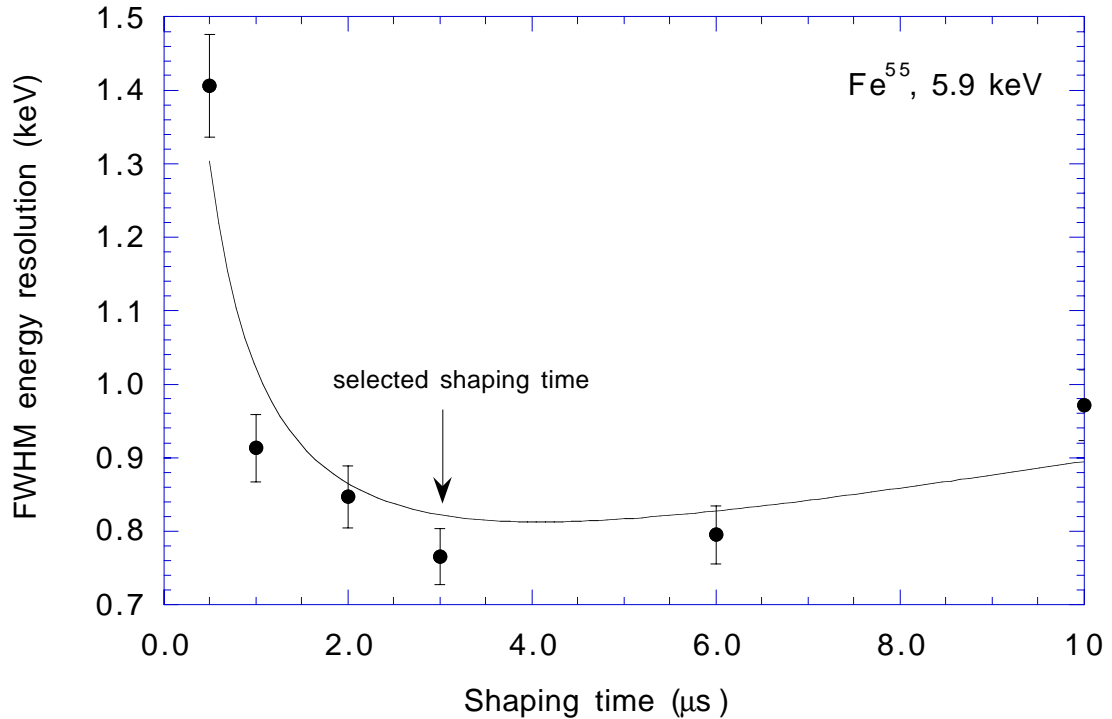


Figure 2. The variation of fwhm energy resolution with shaping time measured at 5.9 keV using an Fe^{55} radioactive source. The solid line shows the expected variation. The detector temperature was -35°C and the bias voltage -40 V .

Before beginning X-ray measurements, the sensitivity of the device, in terms of its charge collection efficiency and energy resolution was evaluated as a function of detector bias using alpha particles from an Am^{241} radioactive source. The bias was varied between -25V and -50 V and the peak channel of the 5.5 MeV alpha peak measured. The peak position was found to vary weakly with bias - the percentage change being $6 \times 10^{-2} V_{\text{bias}}$. For X-rays, no significant change in peak position was found for biases below -40 V . Similarly, the energy resolution did not change significantly. Therefore, in all following measurements the bias was set to -40 V . The temperature dependence was assessed between -40°C and -10°C . As expected, the performance improved with lower temperature especially at the lower energies, so the temperature was kept at -35°C for all subsequent measurements. Lastly, by comparing the response of the detector with a Si detector, the charge collection efficiency (CCE) was estimated to be in the range 90-100%. The calculated CCE using a Monte-Carlo code (see section 4) is 97%, in good agreement.

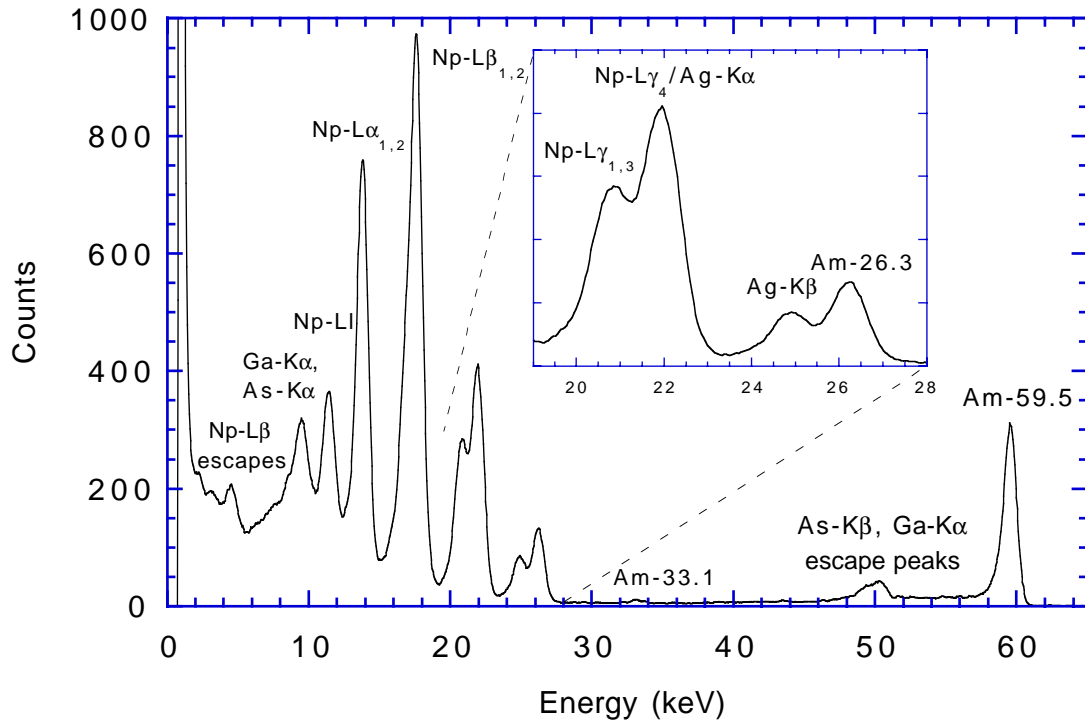


Figure 3. The high energy response of the detector obtained with a Am^{241} source using full illumination. The excellent energy resolution is apparent, being 950 eV fwhm at 59.5 keV. The inset shows the detector's ability to resolve the Np-L γ / Ag K α and Ag K β /Am complexes.

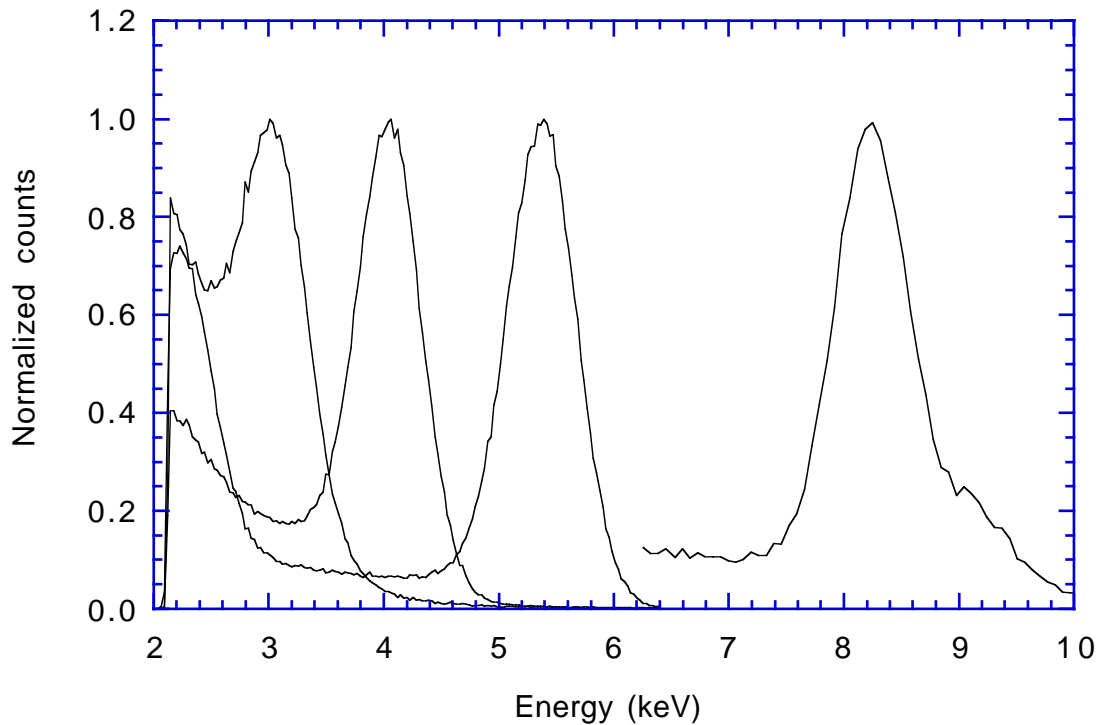


Figure 4. The low energy response of the detector using full illumination (8.0 keV - lab) and a 300 μm pencil beam (3.0, 3.9 and 5.4 keV - BESSY). The noise floor for the BESSY measurements was 2 keV and 1.5 keV for the lab measurements. Note the high energy shoulder on the 8.04 keV line is due to unresolved K β emission at 8.9 keV.

3. Results

The global X-ray response of the detector can be seen in Figure 3 in which we show a spectrum resulting from uniform illumination of an Am^{241} source. The low energy threshold is set by the leakage current at 1.7 keV. The fwhm energy resolution and detection efficiency for the principal line at 59.5 keV are 924 eV and 4.5%, respectively. The energy resolution is such that the L edge sequence of Np lines can be clearly resolved. The additional lines near the Np-L γ complex and the Am^{241} 26.3 keV line are due to Ag K α and K β fluorescence. Ag is used in the packaging of the source and detector. The inset in the Figure shows a close-up of this region.

The low energy response of the detector is given in Figure 4 in which we show an overlay of monoenergetic energy-loss spectra measured at the BESSY electron storage ring (3.0, 4.0 and 5.4 keV), and a Cu fluorescent target source (8.0 keV). The BESSY measurements were carried out using a 300 μm diameter pencil beam at the center of the detector. The Cu measurement was carried out under full uniform illumination. From the figure it can be seen that the photopeak responses can be well approximated by a Gaussian and the continuum by a constant level. The response at the lowest energies is dominated by the leakage current which can be approximated by an exponential function. The high energy shoulders on the 8.0 keV Cu line is due to unresolved K β emission at 8.9 keV. The typical energy resolution recorded at these energies was ~ 800 eV fwhm and the broadening due to electronic noise 370 eV fwhm. This implies that the Fano limited energy resolution must be $< \sim 600$ eV (see section 3.2). There was no apparent difference between the fwhms recorded with the pencil beam and full illumination. We attribute this to increased noise encountered at the BESSY facility. In fact the noise floor was measured to be ~ 2 keV at BESSY as opposed to ~ 1.5 keV in the lab.

3.1. Linearity

Using a variety of lines from 6 fluorescent target sources (Cu, Rb, Mo, Ag, Ba and Tb) and 2 radioactive sources (Fe^{55} and Am^{241}), the detector linearity curve was measured using uniform illumination at an operating temperature of -35°C and is shown in Figure 5. The non-linearity was determined from the residuals of a best-fit linear regression ($\chi^2 = 14$ for 15 degrees of freedom) to the measured line center energies ranging from 2 to 60 keV. It was found to be at worst 1% across the usable energy range.

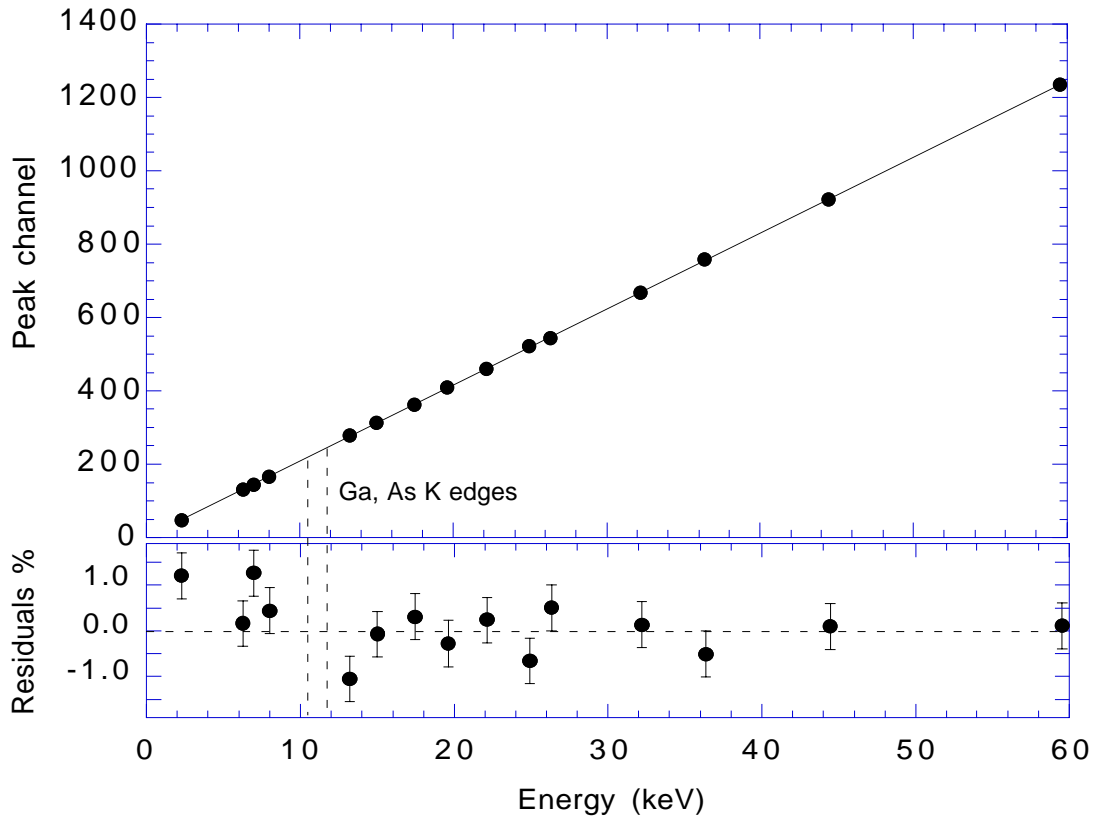


Figure 5. The measured linearity of the detector under full illumination. The lower panel shows the residuals, i.e., the percentage deviation from the best linear fit (measured-calculated / calculated \times 100). The vertical dotted lines indicate the Ga and As K absorption edges at 10.4 and 11.9 keV, respectively.

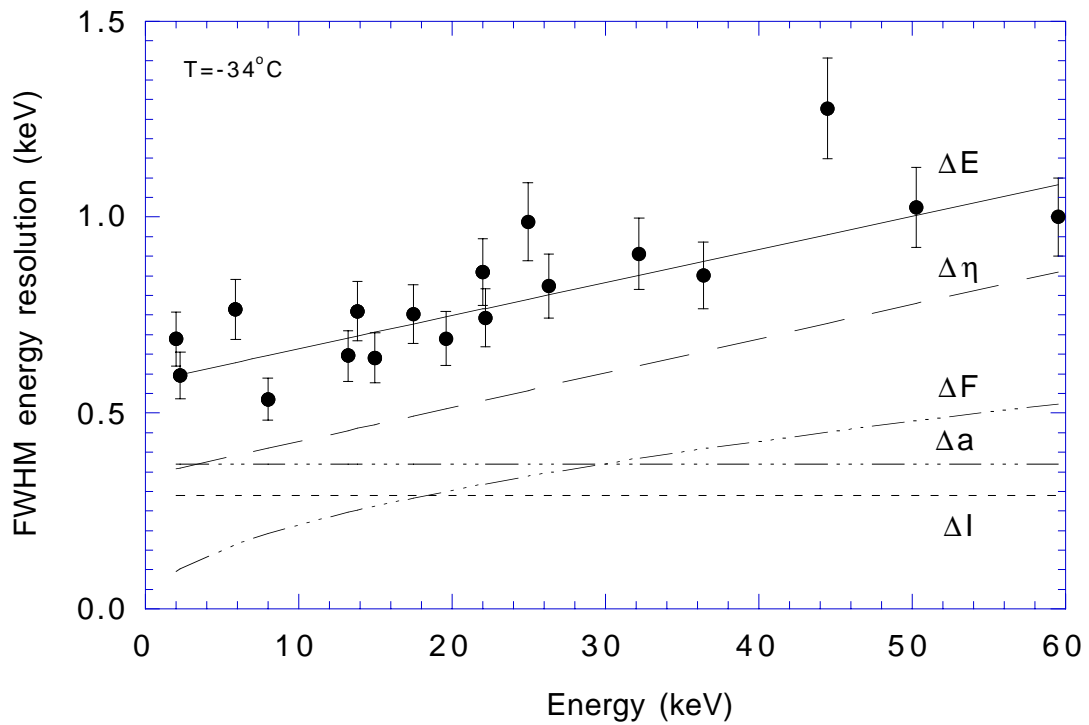


Figure 6. The measured energy resolution under full uniform illumination. The solid line shows the best-fit resolution function to the combined data set. The individual components of the FWHM are also shown: these are noise due to carrier generation or Fano noise, ΔF , reverse current or leakage current noise, ΔI , amplifier shot noise, Δa , and incomplete charge collection noise, $\Delta\eta$.

A plot of the residuals is shown in the lower panel of Figure 5. Above the As and Ga K-edges (indicated by the vertical dotted lines) the residuals show no systematic trend with energy with a mean deviation of $(0.1 \pm 0.47)\%$. However, the residuals below the K-edges are systematically higher with a mean value of 0.51%.

3.2. Energy resolution

The measured energy resolution of the system is shown in Figure 6 along with the calculated resolution from which we see there is good agreement. For completeness, the individual components are also shown which were determined as follows. For small GaAs detectors, one need only consider only 4 components of noise:

a) Noise resulting from the statistical nature of the charge generation whose variance is given by

$$\sigma_F^2 = F\varepsilon E \quad (keV)^2 \quad (1)$$

where F is the Fano factor [5] which describes the fluctuations in ionization and ε is the energy to release an electron-hole pair. For GaAs, $F=0.18$ [6] and $\varepsilon=4.6$ eV [7].

b) Shot noise associated with the leakage current, I , of variance

$$\sigma_I^2 = I\tau\varepsilon^2 A / e \quad (keV)^2 \quad (2)$$

where e is the electronic charge, A is a constant depending on the type of signal shaping and τ is the shaping time. For the Gaussian shaping typically used in spectroscopy, $A = 0.875$.

c) Amplifier shot noise of variance σ_a^2 $(keV)^2$ which depends on the actual design and specifically the capacitive loading of the front end electronics.

d) Noise due to the incomplete charge conversion, characterised by a fwhm Δ_η .

Components a) and b) were calculated and c) measured using a pulser. In analogy with Ge detectors [8], component d) was assumed to have a linear dependence of the form

$$\sigma_\eta^2 = a_1 + a_2 E \quad (keV)^2 \quad (3)$$

The expected resolution function is thus

$$\Delta E = 2.35 \sqrt{\sigma_F^2 + \sigma_I^2 + \sigma_a^2 + \sigma_\eta^2} \quad (keV) \quad (4)$$

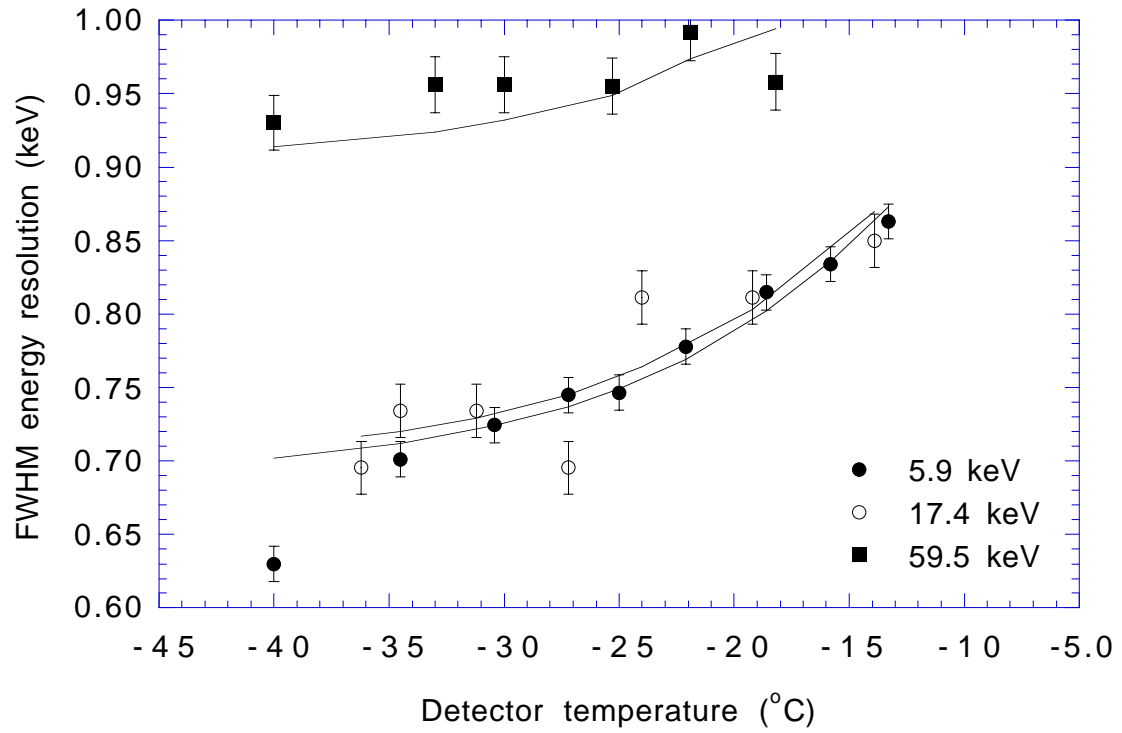


Figure 7. The variation of fwhm energy resolution at 5.9, 17.4 and 59.5 keV as a function of detector temperature. The solid lines show the calculated variation.

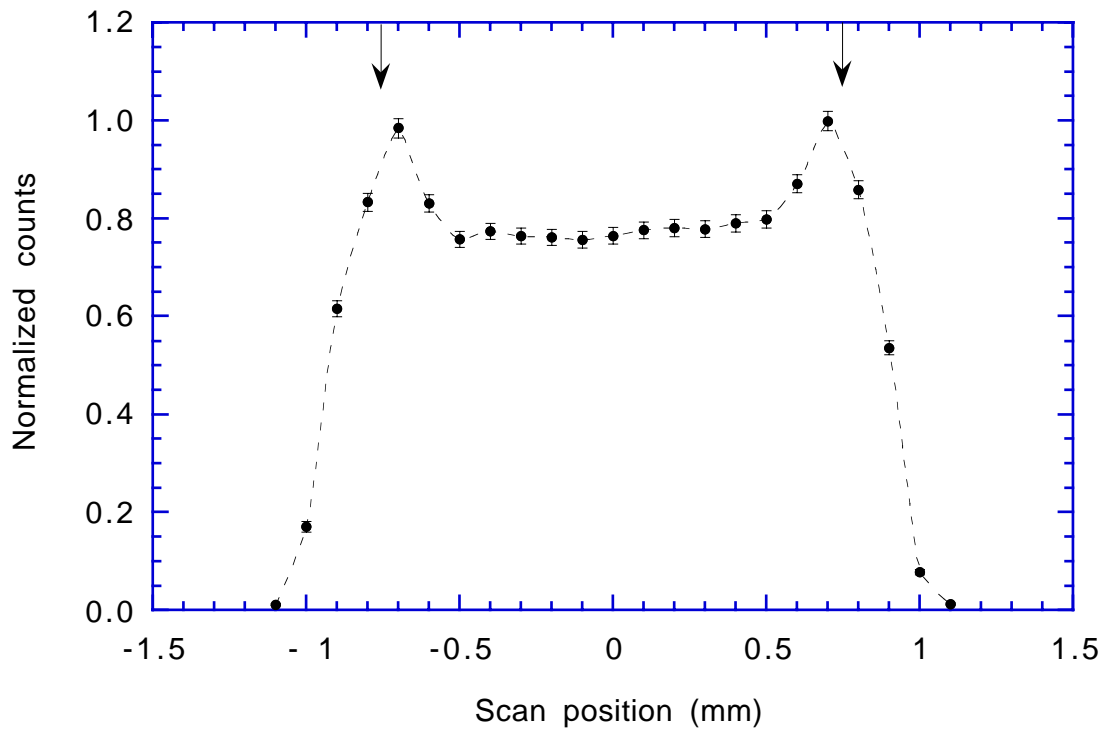


Figure 8. The variation of count rate across the detector averaged over two perpendicular axis. The photon energy is 4 keV, the step size 0.1 mm and beam aperture 0.3 mm. The detector boundaries are indicated.

At a bias of -40V and T=-34°C, the best fit free parameters a_1 and a_2 were 0.1443 and 3.71×10^{-3} keV, respectively. The calculated resolution and the individual components are plotted in Figure 6 from which we can see that the resolution varies slowly with energy and is dominated by electronic and leakage current shot noise below ~5 keV and noise due to incomplete charge conversion above.

In Figure 7 we plot the fwhm energy resolution measured as a function of temperature at incident energies of 5.9, 17.4 and 59.5 keV. In all cases, the resolution improves with decreasing temperature, although the effect gets progressively smaller with increasing energy. In fact the percentage change in ΔE is ~0.81, 0.66 and 0.17% per °C for incident energies of 5.9, 17.4 and 59.5 keV, respectively. At each energy, the decrease in resolution is largely due to a reduction of the leakage current with temperature and to a much lesser extent, the freezing out of traps. The leakage current, I , varies with temperature, T as

$$I = A^* T^2 e^{-e\Phi/kT} \quad (5)$$

where, A^* is a constant related to Richardson's constant, Φ is the barrier height of the Schottky contact and k is Boltzmann's constant. The solid lines in Figure 7 show the calculated temperature dependence based on Eqs 2, 4 and 5 and using a best-fit value of Φ of (0.51 ± 0.02) eV. This value is consistent with those measured for similar sized detectors [9]. The contribution due to the freezing out of traps was evaluated using the Monte-Carlo code described in Section 4 and determined to be negligible in this temperature range, - specifically <6% of the variation due to the leakage current. Note that the variation of ΔE with T is less pronounced at the higher energies. This is because the current noise component forms a smaller fraction of the total fwhm at these energies.

3.3. Spatial response

The spatial response of the detector was evaluated at BESSY using a collimated beam of size 300 μm diameter. Figure 8 shows the count rate profile across the detector averaged across mutually perpendicular axis, normal to the surface. The energy of the scan is 4 keV and the step size 0.1 mm. It is found that the count rate response within the central 1 mm of the detector is constant within a few percent and is consistent with both the statistical errors and the expected variation due to the non-uniformities in the thickness of the p+ layer ($\sim \pm 0.2\mu\text{m}$). However, the response within ~0.2 mm of the edge begins to rise and is enhanced by ~ 20% at the edge. This is much greater than the error of individual measurements (~1.4%). Its rise and shape are due to transmission through the 1 mm wide etch ring in the dead layer separating the mesa and guard ring, convolved

with the beam size. The response then falls off linearly at the edge, consistent with the expected vignetting of the incident beam. Assuming that additional charge loss mechanisms acting immediately at the detector boundary are negligible, we can deduce the thickness of the dead layer by the difference in transmission immediately before and after the mesa. We calculate a thickness of $(6.1 \pm 0.3) \mu\text{m}$. The error is purely statistical.

4.0 Detector modelling

The detector response and the efficiency for detecting events has been evaluated using a Monte-Carlo code [10] based on the Hecht model [11]. The model includes the effects of charge trapping and detrapping and allows the electric field geometry to be altered to reflect field distortion at the edges and weak field regions near the metalization contacts (eg. see [2,12]). The initial electron/hole trapping parameters used in the model (e.g., energy levels, densities, capture cross sections, etc) were typical values determined by deep level transient spectroscopy [10]. Seven traps and/or trap complexes were considered. These values were then 'fine-tuned' by best fitting the Am^{241} spectrum given in Figure 3. In Figure 9 we show a comparison of the best simulated spectra with the experimental data from which we can see there is good agreement. It was found that the spectrum was particularly sensitive to both the density of traps and the overall cross-

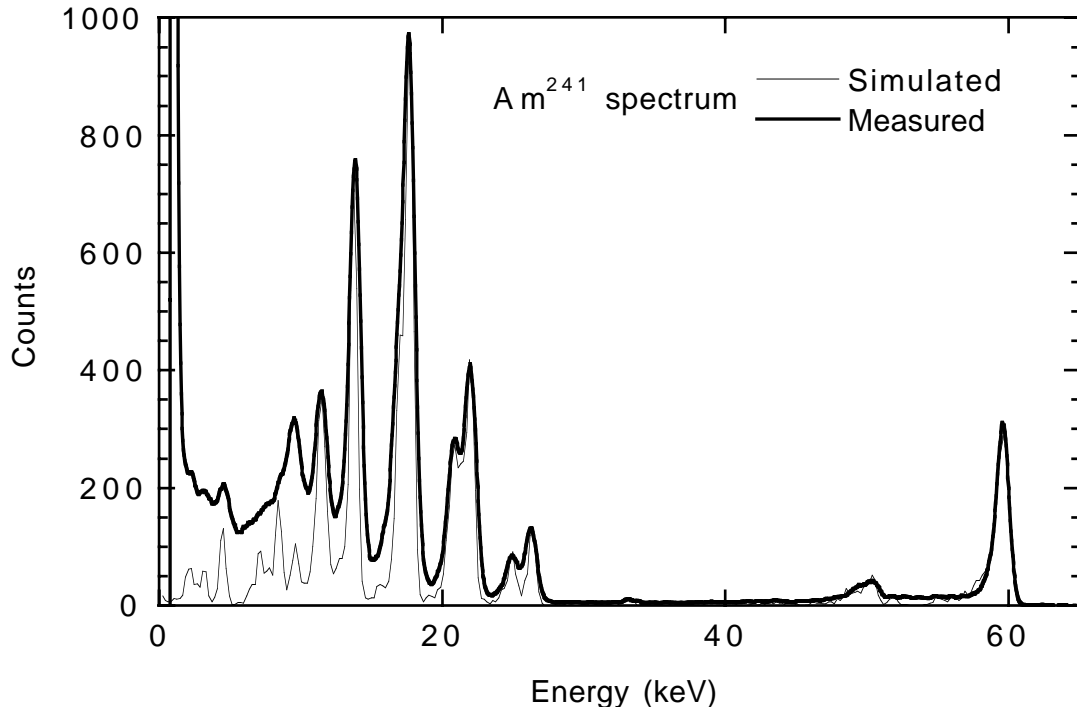


Figure 9. Comparison of a Monte-Carlo simulated Am^{241} energy-loss spectrum and the experimental spectrum. The deviations at low energies are caused by charge loss at the detector boundaries due to non-uniformity of the electric field at the edges.

sections. The best fit cross section-density products (σN) were 7.0 cm^{-1} for electrons and 3.0 cm^{-1} for holes. These values are low and indicate the material used to fabricate the detector was of excellent quality. The rise in continuum at low energies is due to a combination of charge loss resulting from field distortion at the detector edges and preferential electron trapping in the low field region near the ohmic contact. In contrast we attribute the low energy tailing at high energies to preferential hole trapping. The large differences between the simulated and measured spectra at low energies is due to model limitations. Specifically, modelling the charge loss which results from a build up of space charge near the Schottky contact and non-uniformities in the electric field near the detector edges. Lastly, based on our model, Figure 10 shows the calculated detection efficiency, ϵ_{eff} , from which we can see the detector has a usable energy range from 3-60 keV (we arbitrarily define this, as the range for which $\epsilon_{\text{eff}} > 5\%$).

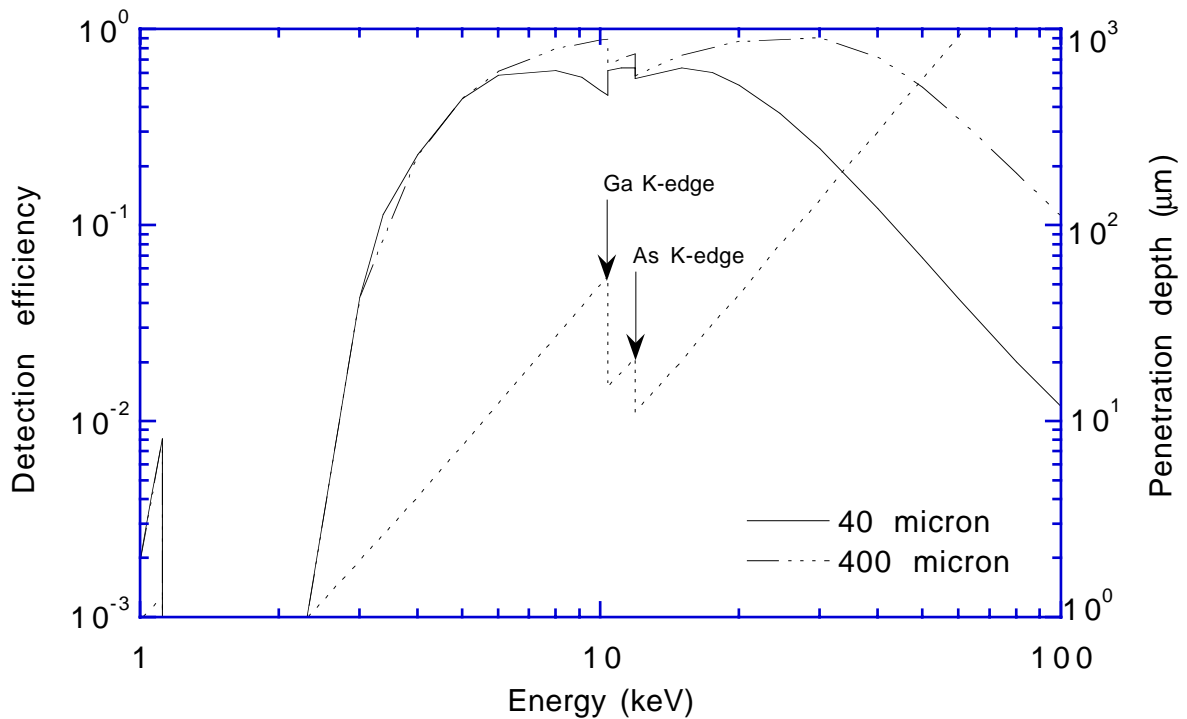


Figure 10. The calculated X-ray detection efficiency. The penetration depth in GaAs is also shown by the dotted line (right hand ordinate). For interest, we also show the expected improvement in efficiency if the depletion depth is increased by a factor of 10 to $400\mu\text{m}$. Such a detector has been fabricated and is undergoing tests.

5. Discussion and conclusions

This detector yields some of the best performance figures yet reported for full beam illumination [e.g. 13,14]. For example the best energy resolution attained was 630 eV at 5.9 keV and 920 eV at 59.5 keV at a modest detector temperature of $-40 \text{ }^\circ\text{C}$. This should be compared to the calculated Fano resolutions of 150 eV and 550 eV at the same

energies. The temperature dependent energy resolution indicates that the low energy (< 4 keV) detector response is dominated by the leakage current and a combination of leakage current and trapping noise at the higher energies. This and the low energy tailing of lines could be improved by increasing the detector bias. At present, however, the maximum bias that can be applied is -80V at -35°C . A substantially higher bias would only be viable with a higher crystal purity and very low impurity concentrations ($\ll 10^{14}$ atoms cm^{-3}). Recently, Bertuccio et al. [15] have shown that charge collection efficiencies (CCE) higher than 98% are required to reduce the effects of trapping noise to a level where it becomes comparable with electronic and Fano noise. Our Monte-Carlo code predicts CCEs near 97%, which is tantalisingly close.

Finally, pulse shape discrimination (PSD) could be used to improve spectra, but at the expense of rejecting valid events - by as much as 50% in the present experimental arrangement. In this case, PSD would negate the advantage of higher z material compared to silicon.

Acknowledgements

We thank T. Tuomi, K.T. Hjelt and M. Juvonen for their contributions to this project and Alex Short for providing the Monte Carlo code and useful discussions.

References

- [1] C.M. Buttar, Nucl. Instr. and Meth. A395 (1997) 1.
- [2] D.S. McGregor and J.E. Kammeraad, in Semiconductors and Semimetals, Academic Press, New York, 43 (1995) 393.
- [3] M. Bavdaz, S. Kraft, A. Peacock, F. Scholz, M. Wedowski, G. Ulm, S. Nenonen, M.A. Gagliardi, T. Gagliardi, T. Tuomi, K.T. Hjelt, M. Juvonen, in Semiconductors for Room Temperature Radiation Detector Applications II, eds. R. James, T. Schlesinger, P. Siffert, W. Dusi, M. Squillante, M. O'Connell and M.Cuzin, Materials Research Society Symposium Proceedings Vol 487, Materials Research Society, Pennsylvania, 565 (1997).
- [4] J. Feldhaus, F. Schafers and W. Peatman, Proc. SPIE, 733 (1986) 242.
- [5] U. Fano, Phys. Rev. 72 (1947) 26.
- [6] J.E. Eberhardt, R.D. Ryan and A.J. Tavendale, Nucl. Instr. and Meth. 94 (1971) 463.
- [7] G.T. Wittry and D.F. Kyser, J. Appl. Phys. 36 (1967) 1387.
- [8] A. Owens, Nucl. Instr. and Meth. A238 (1985) 473.

- [9] T.J. Sumner, S. F. Grant, A. Bewick, J. Li, K. Smith and S. Beaumont, Nucl. Instr. and Meth., A322 (1992) 514.
- [10] A. Short, PhD thesis, The University of Leicester, 1997.
- [11] K. Hecht, Z. Phys. 77 (1932) 235.
- [12] A. Castaldini, A. Cavallini, L. Polenta, C. Canali and F. Nava, Nucl. Instr. and Meth. A410 (1998) 79.
- [13] G. Bertuccio, A. Pullia, J. Lauter, A. Foster, H. Luth, IEEE Trans. Nucl. Sci. 44 (1997) 1.
- [14] T.J. Sumner, S.M. Grant, D. Alexiev, K.S.A. Butcher, Nucl. Instr. and Meth. A348 (1994) 518.
- [15] G. Bertuccio, C. Canali and F. Nava, Nucl. Instr. and Meth. A410 (1998) 29.